HAL
archives-ouvertes.fr

Refining the 3D surface of blood vessels from a reduced set of 2D DSA images

Erwan Kerrien, Marie-Odile Berger, Jérémie Dequidt

▶ To cite this version:

HAL Id: inria-00321550
https://hal.inria.fr/inria-00321550

Submitted on 15 Sep 2008

Refining the 3D surface of blood vessels from a reduced set of 2D DSA images

Erwan Kerrien[1], Marie-Odile Berger[1], and Jérémie Dequidt[2]

[1] Magrit project-team, INRIA Nancy-Grand Est/LORIA, France,
{Erwan.Kerrien,Marie-Odile.Berger}@loria.fr
[2] Alcove project-team, INRIA Lille-Nord Europe/LIFL, France,
Jeremie.Dequidt@lifl.fr

Abstract. Numerical simulations, such as blood flow or coil deployment in an intra-cranial aneurism, are very sensitive to the boundary conditions given by the surface of the vessel walls. Despite the undisputable high quality of 3D vascular imaging modalities, artifacts and noise still hamper the extraction of this surface with enough accuracy. Previous studies took the a priori that a homogeneous object was considered to make the reconstruction from the Xray images more robust. Here, an active surface approach is described, that does not depend on any particular image similarity criterion and grounds on high speed computation of the criterion derivatives. Mean square error and normalized cross-correlation are used to successfully demonstrate our algorithm on real images acquired on an anthropomorphic fantom. Preliminary results of coil deployment simulation are also given.

1 Introduction

An intracranial aneurism is a localized blood-filled dilation of a blood vessel that may occasionally rupture, causing hemorrhage, stroke or death. Medical treatment consists in excluding the aneurism from blood circulation either by surgical clipping or endovascular coil embolization. The latter, more recent, interventional technique is associated with an overall lower morbidity and mortality than surgery (9.5% at one year, compared to 12.2%). Furthermore, the recovery period following the intervention is short and very small aneurisms can be treated (down to 2 mm in diameter). However, the technical challenges that coil embolization faces remain important. It is believed that the still high recurrence rate after treatment would be reduced if the coil dimensions (loop diameter and length) were easier to choose, and coil placement and packing density could be better planned to ensure no blood circulates in the aneurism poach at the end of the treatment. This clearly emphasizes the need for simulation systems that can be used for physician training as well as for pre-operative planning.

Numerical simulations, such as blood flow or coil deployment in an intracranial aneurism, are very sensitive to the boundary conditions given by the surface of the vessel walls. This surface should be smooth to ensure the microtools glide

in a realistic way within the vasculature, and it should be accurate for the simulation to be as exact as possible. Despite the undisputable high quality of 3D vascular imaging modalities, artifacts and noise still hamper the extraction of this surface: blood flow artifacts in magnetic resonance angiography (MRA), tomographic artifacts in computed tomography angiography (CTA) and three-dimensional rotational angiography (3DRA), patient motion induced artifacts in all 3 modalities. Besides, digital subtracted angiography (DSA) remains the modality of reference when a very high precision is required, but it is limited to 2D images.

The work described in this paper aims at refining the surface of the vasculature extracted from any above 3D modality [1], so that this surface is accurate and smooth enough for subsequent simulations. The proposed approach is based on a deformable surface model whose internal force controls smoothness, and which evolves as an active surface until its Xray projections fit the DSA images. A steady streamline of works can be tracked back to the 90's [2] that aimed at making the tomographic reconstruction process more robust to noise and limited data by assuming that a finite set of homogeneous objects is to be reconstructed. Such works followed two main branches. A rather recent branch investigated the use of level-sets to model the object surface. However, this approach was only used for reconstructions from a dense number of views [3,4]. Most works model the object as a polyhedral surface, whose vertex positions are estimated in a Bayesian framework [5,6,7,8]. Free-form deformations [6,7] were also proposed to solve topological issues that could occur e.g. after collisions. This classical framework relies on the Mean Square Error (MSE) criterion, which is not always applicable in practice, since the raw density images are not readily available. Furthermore, optimization requires many derivations of the X-ray projection of the triangulated surface, which is time consuming. Both issues prevented any of these previous studies [6,7,8] from demonstrating their work on real images involving large surface models (thousands of voxels). Section 2 extends the classical framework to other iconic image similarity measures. Analysis of the X-ray projection then allows for insights to speed up the computation of derivatives. Such improvements enable us to demonstrate the global method onto real X-ray images, and give preliminary coil simulation results in section 3.

2 Method

2.1 Active surface model

The input of our refinement algorithm is a triangulated surface V of the vessels. This surface may have several connected components, all closed and oriented. Registered Xray images are assumed to be available, showing the object alone on a uniform background. Section 3 will give details on how these conditions are met in practice with vascular images.

The method we use originates in [9]. The mesh can be viewed as a dynamic system of particles that undergoes external forces F_{ext} and is constrained by

internal forces F_{int}. The Newtonian law of motion is applied on each vertex v_i:

$$m\ddot{v}_i + \gamma\dot{v}_i = F_{int}(v_i) + F_{ext}(v_i) \qquad (1)$$

where m is the mass of the vertex and γ the damping (viscosity) factor. We used a simpler version of F_{int} than [9], namely $F_{int}(v_i) = \alpha(v_i - \bar{v}_i)$, where $\bar{v}_i$ is the average of all neighbours of v_i and α a weight. This force relates to a curvature constraint.

We also set the common particle mass m to null. This has little impact on the convergence of the dynamic system. Then equation 1 leads to a linear system:

$$(A + \gamma I)V^{t+1} = F_{ext}(V) + \gamma V^t \qquad (2)$$

where $A + \gamma I$ is a sparse matrix which is iteratively inverted.

When image data are 3D, external forces are classically expressed as the 3D gradient of the image, which comes from the derivative of an energy expressed as the square gradient norm. Similarly, we consider an external energy term based on an image similarity criterion C (to be minimized):

$$F_{ext}(v_i) = \beta \sum_{D \in \mathcal{D}} \frac{\partial C(\mathbb{P}_D(V), D)}{\partial v_i}$$

where $\mathcal{D}$ is the set of Xray images and $\mathbb{P}_D(V)$ is the Xray projection of the surface under the same incidence as Xray image D, and β a weight. C is traditionnally the Mean Square Error (MSE) [7,6,8]: $C = \sum_D \|\mathbb{P}_D(V) - D\|^2 / N_p$ (N_p is the number of pixels). We shall also consider in the following experiments the Normalized Centered Cross-correlation (NCC):

$$C = 1 - \sum_D E[\mathbb{P}'_D(V)D'] / (\sigma(\mathbb{P}'_D(V))\sigma(D'))$$

with E the expectancy and, for a given image I, $\bar{I}$ its mean, $I' = I - \bar{I}$, the centered image and $\sigma(I')$ its standard deviation.

2.2 Computation of the external force - Surface Xray projection

Computing the external force implies computing the derivatives of C with respect to each v_i. This computation is classically done numerically by using the central difference approximation:

$$\frac{\partial C(\mathbb{P}_D(V), D)}{\partial v_{i,j}} \approx \frac{C(\mathbb{P}_D(V + \delta_{i,j}), D) - C(\mathbb{P}_D(V - \delta_{i,j}), D)}{2\delta}$$

where $v_{i,j}$ is the jth component ($j \in [1, 3]$) of vertex v_i and $V + \delta_{i,j}$ (resp. $V - \delta_{i,j}$) is the surface V perturbed by adding (resp. subtracting) δ to $v_{i,j}$.

This requires computing many Xray projections of the surface, which is time consuming. Soussen [8] derived analytic expressions of the derivative of $\mathbb{P}_D(V)$ but only in the case of parallel projection. This result is not applicable to our case, since DSA images are acquired under central projection geometry. Nevertheless, we demonstrate here how to speed up the Xray projection of a triangulated surface and perform fast numerical computation of the external force.

Xray projection of the surface The triangulated surface V is composed of a finite set of connected components. Each component is closed and oriented. We further assume in what follows that the surface is a topological open: a ray tangent to the surface will be considered as passing outside the surface, so that a ray intersects a triangle at 0 or 1 point.

For a given pixel (u, v), the ray from that pixel to the focal point O_D intersects the surface at an even number of points $(P_k)_{k \in [0, 2M-1]}$ such that the ray enters the surface at P_{2i} and goes out of the surface at P_{2i+1}. We say that P_{2i} is an *entry point* and P_{2i+1} is an *exit point* (see fig. 1, left). The Xray projection of the surface is then given by: $\mathbb{P}_D(V)(u, v) = \sum_{i=0}^{M-1} \|P_{2i+1} - P_{2i}\|$ Since all the intersection points are aligned with O_D, this can be rewritten as:

$$\mathbb{P}_D(V)(u, v) = \sum_{k=0}^{2M-1} \sigma_k \|P_k - O_D\|$$

where $\sigma_k = -1$ if P_k is an entry point and $\sigma_k = 1$ if P_k is an exit point. Each intersection point and thereby each triangle can thus be processed independently. Furthermore, The σ coefficient will be the same for all points on a given triangle t, depending only on the way t is seen from the focal point: Each triangle t can therefore be qualified as either entry, exit or tangent triangle depending on $\sigma(t) = \text{sign}(n_t^T(\bar{t} - O_D))$, with n_t the normal to t (exponent T is for transposition) and $\bar{t}$ its center of gravity. As a result, the Xray projection can be expressed as:

$$\mathbb{P}_D(V) = \sum_{t \in V} \sigma(t) \mathbb{P}(t) \tag{3}$$

Special cases A ray may occasionnally stab an edge or a vertex of a triangle. For the edge case (fig. 1, middle), if both triangles sharing the edge are entry (resp. exit) triangles, the intersecting point is an entry (resp. exit) point. Otherwise, the ray is tangent (no intersection). For the vertex case (fig. 1, right), all triangles sharing this vertex (so-called the *vertex fan*) are projected on the image plane. Each triangle projects onto another triangle. The sum of the oriented angles at the common summit in the projected fan is either 2π for an entry point, -2π for an exit point or 0 in the tangent case.

Degenerate cases occur when one of the involved triangles is tangent to the ray. The full triangle case is trivial since no intersection occur. The edge and vertex cases are resolved using Simulation of Simplicity (SoS) [10]: one (edge case) or two (vertex case) vertices of the tangent triangle are moved by $-\epsilon n_t$ (with $\epsilon > 0$). The status of the intersecting point can then be set and does not depend on ϵ (the proof is too long to hold on this paper).

Computation of the external forces Computing the external forces implies updating the Xray projection of the surface after a single vertex v_i was moved by δv. The motion only changes the vertex fan of v_i. Following equation 3, this update can be made by subtracting the projection of the vertex fan of v_i, moving
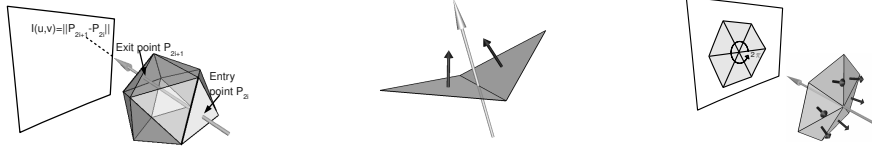
Fig. 1. Xray projection: (left) a ray intersects the surface at an even number of points: each entry point corresponds to an exit point. (middle) An exit edge connects 2 exit triangles; (right) entry vertex: the sum of the angles on the projected fan is 2π. (White arrow: Xray direction, black arrows: outward face normals.)

v_i and adding the projection of the new vertex fan:

$$\mathbb{P}_D(V') = \mathbb{P}_D(V) - \sum_{t \in \mathcal{V}_i} \sigma(t)\mathbb{P}_D(t) + \sum_{t' \in \mathcal{V}'_i} \sigma(t')\mathbb{P}_D(t')$$

where $\mathcal{V}_i$ is the vertex fan of v_i, $\mathcal{V}'_i$ is the new vertex fan and V' the surface after the vertex motion. This computation only involves a few triangles and concerns a few pixels in the image. The update of the similarity criterion is therefore very fast, leading to a fast computation of the central difference scheme.

3   Results

The whole algorithm was implemented in C++ based on the open source Gnu Triangulated Surface library (GTS) (`http://gts.sourceforge.net`). For all the experimentations, the following common configuration was chosen: the surface was retriangulated each 10 iterations; for the numerical derivation $\delta = 2$. The only varying parameters were: number of iterations; internal coefficient α ; external coefficient β; and viscosity parameter γ.

3.1   Synthetic ellipsoid with MSE

A first synthetic experiment was conducted, taking an ellipsoid with a much larger main axis than the other two (equal) axes, so as to approach the shape of a blood vessel. 3 Xray views were simulated: antero-posterior (AP), lateral and top. The ellipsoid was slightly turned so that its main axis was not exactly aligned with the lateral view direction. The process was initialized with a much thinner ellipse. Indeed, active surfaces naturally tend to shrink. Looking for an enlargement should show up the effects of the external force. 500 iterations were made, with $\alpha = 1$ $\gamma = 10$ and $\beta = 100$. The MSE similarity criterion was chosen. Figure 2 shows some steps in the optimization: the convergence was fast for the occluding vertices, as in classical computer vision cases, but the Xray density information still acted, yet much more slowly, to make the other vertices converge. The shortening of the ellipsoid is to be noted: this is due to much higher internal forces at the extremities where the curvature is very strong.
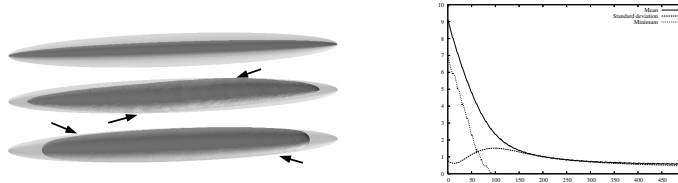
Fig. 2. Synthetic experiments: (left) Screen captures at iteration 0, 100 and 400. The true shape is translucent. The shape first evolves to fit the occluding contours (arrows on the middle image), and then slowly converges on parts where only density information is available. (right) evolution of the distance to the true shape.

3.2 Anthropomorphic phantom

A second experiment was performed on real images of an anthropomorphic phantom of the brain vasculature (Elastrat, Geneva: rigid phantom with 3 aneurisms).

Surface data A 3DRA was acquired on the phantom on an Innova 4100 angiography machine (GE Healthcare: 512^3 voxel data cube, 0.25 mm voxel size) and the vessel isosurface was extracted using the marching cube from the GTS. In the absence of a CAD model, this surface was considered as ground truth. The initial surface was obtained by simulating MRA conditions: the 3DRA volume was subsampled to a voxel size of 1 mm, using nearest neighbour interpolation, and an isosurface extracted using marching cube (10210 vertices).

DSA images 4 DSA sequences were available for the phantom: one AP and one lateral view, as well as two other "working" views, that the physician would have used to treat the aneurism. The bolus density 3D map can be considered constant in the vessels, if averaged over a sufficient time (e.g. arterial time). Due to the linearity of the projection operator, this volume projection is the average of the first DSA images in the sequence: the average over the first 10 images was considered as Xray data. However, since equality cannot be assumed between the real Xray data and the synthetic surface projection, NCC was considered in this experiment. DSA images were registered with the 3DRA volume using [11]. Only crops of about 200×130 pixels around the aneurism were considered to speed up the process. As a result, the optimization concerned 5900 vertices.

Experimentations The algorithm was run in two passes of 100 iterations each: a first step with a very small internal force ($\alpha = 0.001, \gamma = 30, \beta = 60000$) to correct for the larger differences, but preserve the small vessels and a second step to refine the surface and smooth it ($\alpha = 0.03, \gamma = 2, \beta = 10000$). Figure 3 shows the result of the reconstruction: the shape of the aneurism and the largest vessels are well recovered and the surface is even smoother than in the ground truth image. The small vessel surface is however more irregular. Indeed, the internal force is much stronger on small vessels with highly curved cross-section and
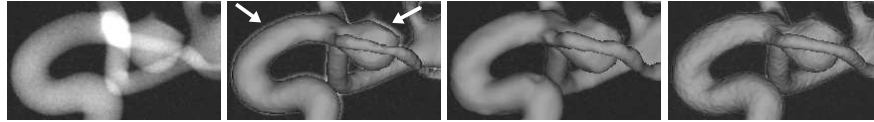
Fig. 3. Experiments on real data: (from left to right) lateral Xray DSA image; initialization: notice the error at the top of the aneurism and vessel boundaries (arrows); final surface: the aneurism surface and the large vessels were recovered, and the surface is smoother than in the ground truth surface; ground truth surface: notice the size of the small vessel before the aneurism is underestimated compared to the DSA image.
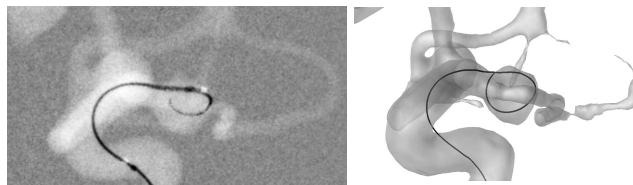

Fig. 4. Simulation of coil deployment: (left) actual coil position, as seen in DSA; (right) simulation of the coil within the vessel surface given by our algorithm.

should be adapted to the local vessel size. 47 minutes were necessary for the 200 iterations. As a comparison, extrapolating Soussen's results [8] to our experiment would require 1470 minutes (350 seconds for 10 iterations, 210 vertices and 9 64×64 images, in parallel projection).

3.3 Simulation of coil deployment

A preliminary experiment to simulate a coil deployment was made using the simulation method presented in [12]. The vessel surface was segmented and refined using our algorithm (see fig. 3). Figure 4 shows the actual coil seen in a DSA image and compares it with the simulated coil within the vessels in a similar orientation to demonstrate a very encouraging realism of the simulation (note that some vessels shrunk because they were not visible in the cropped DSA images).

4 Discussion and future works

Despite tremendous improvements in 3D vascular medical imaging, discrepancies still exist with DSA images that the interventional radiologist uses as feedback to his/her surgical gesture. Such differences could be reduced by a binary object reconstruction method such as [8], let apart 3 main issues that prevent such methods from being applicable on real data: good initialization, since the problem is very ill-posed; appropriate image similary criterion, since the input images are in general known up to a look-up transform; fast computation of the criterion

derivatives, since many vertices are involved in real datasets and many iterations are required.

The work described in this paper proposes to initialize the surface from a 3D vascular imaging modality, extends previous reconstruction works to any image similarity criterion, and describes how derivative computations can be sped up. While previous works were only demonstrated on synthetic data, results are here provided on real datasets of an anthropomorphic phantom. As future work, parameter tuning is not a trivial task, that we expect will be better circumscribed after a more extensive testing on actual patient data. Furthermore, Lachaud's work [9] will be integrated to enable topological changes on the surface, that may be necessary to separate two very close vessels.

As an illustrative example application, preliminary, though very realistic, simulation results are provided for the deployment of a coil within an intracranial aneurism. Other applications can exploit our method, when the 3D vessel needs to updated from a DSA sequence: estimation/correction of blood vessel deformation when the micro-tools are inserted or due to the arterial pulsatility, or blood flow reconstruction in 3D by a 3D bolus tracking approach.

References

1. Kirbas, C., Quek, F.: Vessel extraction techniques and algorithms: A survey. In: Proc. of the 3rd Symp. on Bioinformatics and Bioengineering. (2003) 238–45
2. Bresler, Y., Fessler, J.A., Macovski, A.: A Bayesian approach to reconstruction from incomplete projections of a multiple object 3D domain. IEEE Trans. PAMI **11**(8) (1989) 840–58
3. Bruandet, J.P., Peyrin, F., Dinten, J.M., Barlaud, M.: 3D tomographic reconstruction of binary images from cone beam projections: A fast level set approach. In: IEEE Int. Symp. on Biomedical Imaging - ISBI'02. (2002) 677–80
4. Feng, H., Karl, W.C., Castañon, D.A.: A curve evolution approach to object-based tomographic reconstruction. IEEE Trans. Image Processing **12**(1) (2003) 44–57
5. Milanfar, P., Karl, W.C., Willsky, A.S.: Reconstructing binary polygonal objects from projections: A statistical view. CVGIP: Graphical Models and Image Processing **56**(5) (1994) 371–91
6. Hanson, K.M., Bilisoly, R.L., Cunningham, G.S.: Kinky tomographic reconstruction. In: SPIE Medical Imaging: Image Processing. Volume 2710. (1996) 156–66
7. Battle, X.L., Le Rest, C., Turzo, A., Bizais, Y.: Three-dimensional attenuation map reconstruction using geometrical models and free-form deformations. IEEE Trans. Med. Imag. **19**(5) (2000) 404–11
8. Soussen, C., Mohammad-Djafari, A.: Polygonal and polyhedral contour reconstruction in computed tomography. IEEE Trans. Image Processing **13**(11) (2004) 1507–23
9. Lachaud, J.O., Montanvert, A.: Deformable meshes with automated topology changes for coarse-to-fine 3D surface extraction. Medical Image Analysis **3**(2) (1999) 187–207
10. Edelsbrunner, H., Mücke, E.P.: Simulation of Simplicity: A technique to cope with degenerate cases in geometic algorithms. ACM Trans. Graphics **9**(1) (1990) 66–104
11. Kerrien, E., Berger, M.O., Maurincomme, E., et al.: Fully automatic 3D/2D subtracted angiography registration. In Taylor, C., Colchester, A., eds.: Proceedings of

the Second International Conference on Medical Image Computing and Computer-Assisted Intervention, Cambridge (UK). Number 1679 in Lecture Notes in Computer Science, Springer Verlag (September 1999) 664–671

12. Dequidt, J., Marchal, M., Duriez, C., Cotin, S.: Interactive simulation of embolization coils: Modeling and experimental validation. In: Proceedings of the 11th International Conference on Medical Image Computing and Computer Assisted Intervention, New York. Lecture Notes in Computer Science, Springer Verlag (September 2008) Accepted for publication.